PHYSICAL REVIEW B **96**, 060509(R) (2017)

Pressure-induced superconductivity up to 13.1 K in the pyrite phase of palladium diselenide $PdSe_2$

Moaz A. ElGhazali,[1,2] Pavel G. Naumov,[1,3] Hossein Mirhosseini,[1] Vicky Süß,[1] Lukas Müchler,[4] Walter Schnelle,[1] Claudia Felser,[1] and Sergey A. Medvedev[1,*]

[1]*Max Planck Institute for Chemical Physics of Solids, 01187 Dresden, Germany*

[2]*Institute for Solid State Physics, Technical University Dresden, 01069 Dresden, Germany*

[3]*Shubnikov Institute of Crystallography of Federal Scientific Research Centre "Crystallography and Photonics" of Russian Academy of Sciences, Moscow 119333, Russia*

[4]*Department of Chemistry, Princeton University, Princeton, New Jersey 08544, USA*

(Received 26 June 2017; published 30 August 2017)

The evolution of electrical transport properties, the electronic band structure, and lattice dynamics of $PdSe_2$ is studied under high pressure. The emergence of superconductivity is reported in the high-pressure pyrite-type phase of $PdSe_2$. In this transition-metal dichalcogenide, the critical temperature of superconductivity rapidly increases with pressure up to 13.1 K. *Ab initio* electronic band structure calculations indicate the presence of Dirac and nodal-line fermions in the vicinity of the Fermi energy protected by the pyrite structure symmetry, which can lead to interesting superconducting states. Raman spectroscopy shows a direct correlation between critical temperature and bonding strength of Se-Se dumbbells in $PdSe_2$, underlining the crucial role of bonding for tuning the superconductivity.

DOI: 10.1103/PhysRevB.96.060509

The exploration of the chemical, structural, and electronic parameters of a solid which lead to the appearance or the enhancement of superconductivity is an ongoing topic of intensive research [1]. In transition-metal dichalcogenides (TMDs), a class of compounds known for their unusual electronic properties and rich intercalation chemistry, superconductivity often competes with diverse exotic phases. In such strongly correlated materials, the crystal and electronic structures can be tuned in a wide range by chemical substitution or application of external pressure [2–6].

Originating from the competition between cationic d orbitals and anionic sp levels, TMDs form either two- (2D) or three-dimensional (3D) structures [7,8]. Layered quasi-2D TMDs often exhibit strongly competing effects of charge-density wave formation and superconductivity [2–4]. The nonlayered 3D TMDs with a pyrite structure are close to insulator-metal transition systems, with various magnetic and electrical phenomena ranging from the prototypical antiferromagnetic Mott insulator NiS_2 to the superconducting copper dichalcogenides [9,10]. The characteristic of the pyrite structure is a strong pairing of the chalcogen atoms (X) forming $(X\text{-}X)^{-2}$ dimers. The bond length in these dumbbells is considered as a key parameter controlling the critical temperature (T_c) of superconductivity in the defective pyrite compounds Ir_xSe_2 and $Ir_{0.94-x}Rh_xSe_2$ [5,6]. These materials, however, are affected by disorder due to nonstoichiometry and chemical substitution. In contrast, the application of external pressure is a "clean" tool to tune the interatomic distances.

Here, we study the interplay between the structure, bonding, and electronic properties in $PdSe_2$, featuring a unique crystal structure on the borderline between 2D and 3D structures [7]. The structure of $PdSe_2$ consists of 2D layers of square-planar coordinated Pd [Fig. 1(a)] due to the stabilization of the low-spin diamagnetic configuration of the Pd^{2+} cation [11]. This decrease in symmetry results in a splitting of the e_g levels, so that the eight electrons of Pd^{2+} fill all available d levels through the lower d_{z^2} level. This configuration accounts for the diamagnetic semiconducting properties of $PdSe_2$ at ambient conditions.

A single-crystalline $PdSe_2$ sample was synthesized by the chemical vapor transport of polycrystalline $PdSe_2$ with iodine as the transport agent. For high-pressure electrical resistivity and Raman spectroscopy measurements, a single crystal of $\sim 5\,\mu$m thickness was loaded in a diamond anvil cell with NaCl as the pressure transmitting medium. Further details of our high-pressure experimental technique are described elsewhere [12].

Theoretical calculations were performed within the framework of density functional theory (DFT) as implemented in the VASP program package [13] using the projected augmented wave method [14,15] with a plane-wave cutoff energy of 350 eV. For Brillouin zone integration, we use a $(5 \times 5 \times 5)$ k-point mesh. The structural relaxation was performed until the maximum force on each atom is less than 0.05 eV/Å. The pseudopotentials are chosen such that the $4p$ and $4d$ states of Pd and the $4s$ and $4p$ of Se are treated as valence states. To take into account the van der Waals forces, a set of calculations with different exchange-correlation functionals was performed with the best agreement between experiment and theory provided by the optPBE-vdW functional [16,17]. The Fermi surface is calculated by the WANNIER90 code [18].

Application of pressure systematically changes the transport properties of $PdSe_2$ [Fig. 2(a)]. For pressures below 3 GPa, the temperature dependence of the resistivity $\rho(T)$ shows a semiconducting behavior. The band structure calculation for $PdSe_2$ at ambient pressure [Fig. 3(a)] reproduces the semiconducting properties with an indirect band gap of $\sim$0.25 eV. The room-temperature resistivity rapidly decreases as pressure increases, and $\rho(T)$ above 3 GPa shows metallic behavior, indicating the metallic state in $PdSe_2$. This is in reasonable agreement with the results of band structure calculations showing a band gap closure at about 2 GPa [Fig. 3(b)].

*medvedie@cpfs.mpg.de

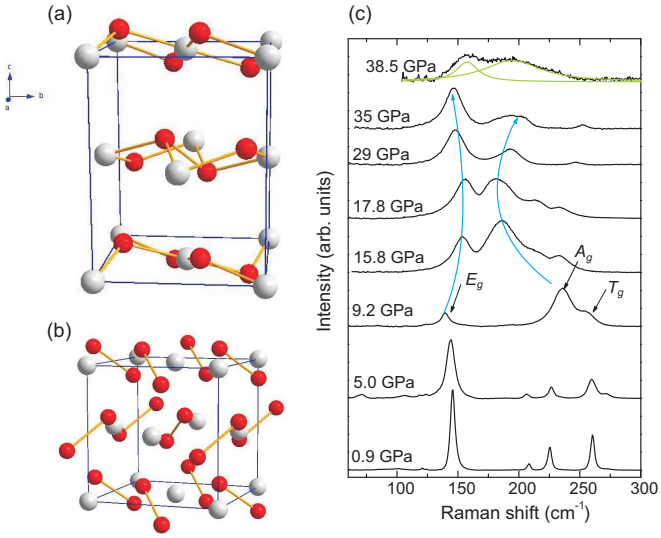

FIG. 1. Crystal structures of $PdSe_2$. The ambient pressure PdS_2-type structure (a) can be described as an elongated pyrite structure, which transforms under pressure (>6 GPa) to the pyrite-type structure [19] (b). The change in the Raman spectra between 5 and 9.2 GPa (c) indicates the structural transition to a pyrite-type structure. The mode assignment within the pyrite structure is shown on the spectrum at 9.2 GPa. Blue arrows schematically show the unusual evolution of the E_g libration and the A_g stretching vibrations of the Se_2 dumbbells with pressure. The pyrite phase of $PdSe_2$ is stable up to 37 GPa, above which the Raman spectrum changes (the green lines for 38.5 GPa show the deconvolution of the observed spectrum into two broad peaks), indicating a structural transition to a next high-pressure phase of $PdSe_2$ referred to as the γ phase.

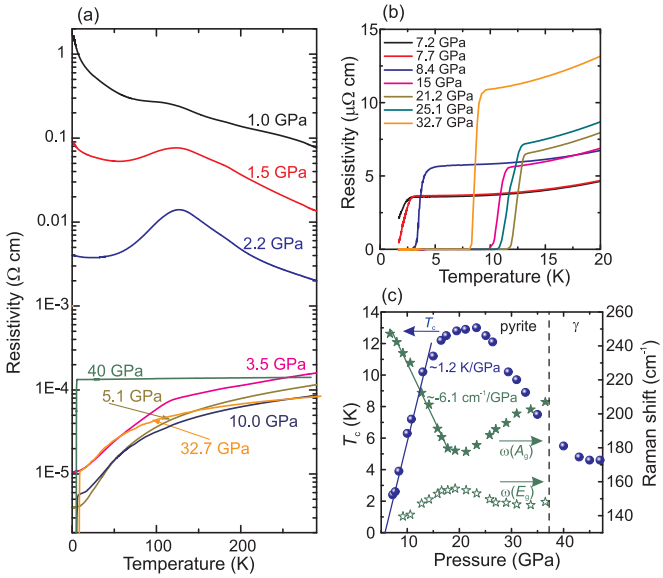

FIG. 2. Pressure evolution of the electronic transport properties of $PdSe_2$. (a) Application of pressure tunes the electronic properties of the PdS_2-type phase of $PdSe_2$ from a semiconductor to a metal at pressures above 3 GPa. (b) With the transition to the pyrite phase, superconductivity emerges with T_c showing a dome-shaped dependence on pressure with a maximum T_c of 13.1 K at $P \sim 23$ GPa. (c) Demonstration of the correlation between the pressure evolutions of T_c and frequencies of internal stretching vibration (A_g mode) and librational (E_g mode) modes of the Se_2 dumbbells. The sudden increase of the room-temperature resistivity at $P = 37$ GPa and the change of the temperature dependence $\rho(T)$ in the normal state [a very weak temperature dependence, as illustrated by the curve at 40 GPa in (a)] indicates a structural transition to the γ phase. The γ phase remains superconducting [curve at 40 GPa in (a)] with T_c weakly depending on pressure.

The metallization occurs without a structural phase transition, as indicated by Raman spectroscopy data [Fig. 1(c)], proving the stability of the PdS_2-type structure up to pressures ≈6 GPa, in full agreement with the structural studies of $PdSe_2$ [19]. At a pressure of 6–10 GPa, $PdSe_2$ undergoes a structural phase transition to a pyrite-type structure [19], indicated by the change of Raman spectra [Fig. 1(c)]. Comparing the Raman spectra of the high-pressure phase of $PdSe_2$ at 9.2 GPa with those of $NiSe_2$ [20], the observed peaks can be well assigned to the E_g librational mode and A_g and T_g in-phase and out-of-phase stretching vibrations of the Se_2 dumbbells [Fig. 1(c)]. The E_g mode is largely governed by the Pd-Se force constant while the frequency of the A_g stretching reflects the strength of Se-Se dumbbell bonding.

The pyrite phase of $PdSe_2$ is clearly metallic [Fig. 2(a)], in agreement with its calculated band structure [Figs. 3(c) and 3(d)]. Two bands with mainly Se p and Pd $d_{x^2-y^2}$ characters cross the Fermi energy (E_F) close to Γ and X (M), respectively, and some other bands have their extrema close to E_F. With further increasing pressure, the latter band extrema move away from E_F [Fig. 3(d)]. This change in the electronic structure causes only a small change in the density of state (DOS) at E_F for different applied pressures [right panels in Figs. 3(c) and 3(d)]. Without spin-orbit coupling (SOC), there are three nodal lines about 0.25 eV above E_F in the $k_x = 0, k_y = 0$, and $k_z = 0$ planes [Fig. 3(c)] allowed by the three mirror symmetries $[M_x|\frac{1}{2}\frac{1}{2}0]$, $[M_y|0\frac{1}{2}\frac{1}{2}]$, and $[M_z|\frac{1}{2}0\frac{1}{2}]$ that are characterized by an MZ invariant [21]. Upon inclusion of SOC, a gap of the order of 0.02 eV opens. There is an additional Dirac crossing along the ΓM direction at slightly higher energies which is unaffected by SOC [Fig. 3(e)]. The topological protection remains in the limit of small gap opening terms such as SOC, as it is the case in $PdSe_2$. Topological nontrivial bulk and surface states attracted much interest recently in context of their interplay with the superconducting instability [22–24]. Interestingly, we find an eightfold degeneracy at the M point at the Fermi level that splits into two fourfold degeneracies separated by ∼0.01 eV if SOC is included [Fig. 3(f)]. These higher-order degeneracies are stabilized by the presence of nonsymmorphic symmetries [25]. Conditioned by the nodal lines and the fourfold degeneracies, the Fermi surface of pyrite $PdSe_2$ consists of a large central pocket and a network connected along the edges of the Brillouin zone [Fig. 3(g)], and is similar to that of metallic NiS_2 just above its insulator-to-metal transition [26].

Most interestingly, at low temperatures a superconducting state emerges in pyrite $PdSe_2$. At a pressure of 7.2 GPa, a drop of the resistivity appears below a temperature of 2.4 K, suggesting the onset of a superconducting transition. The superconducting state is clearly observed at higher pressures with the resistivity dropping abruptly to zero. The critical

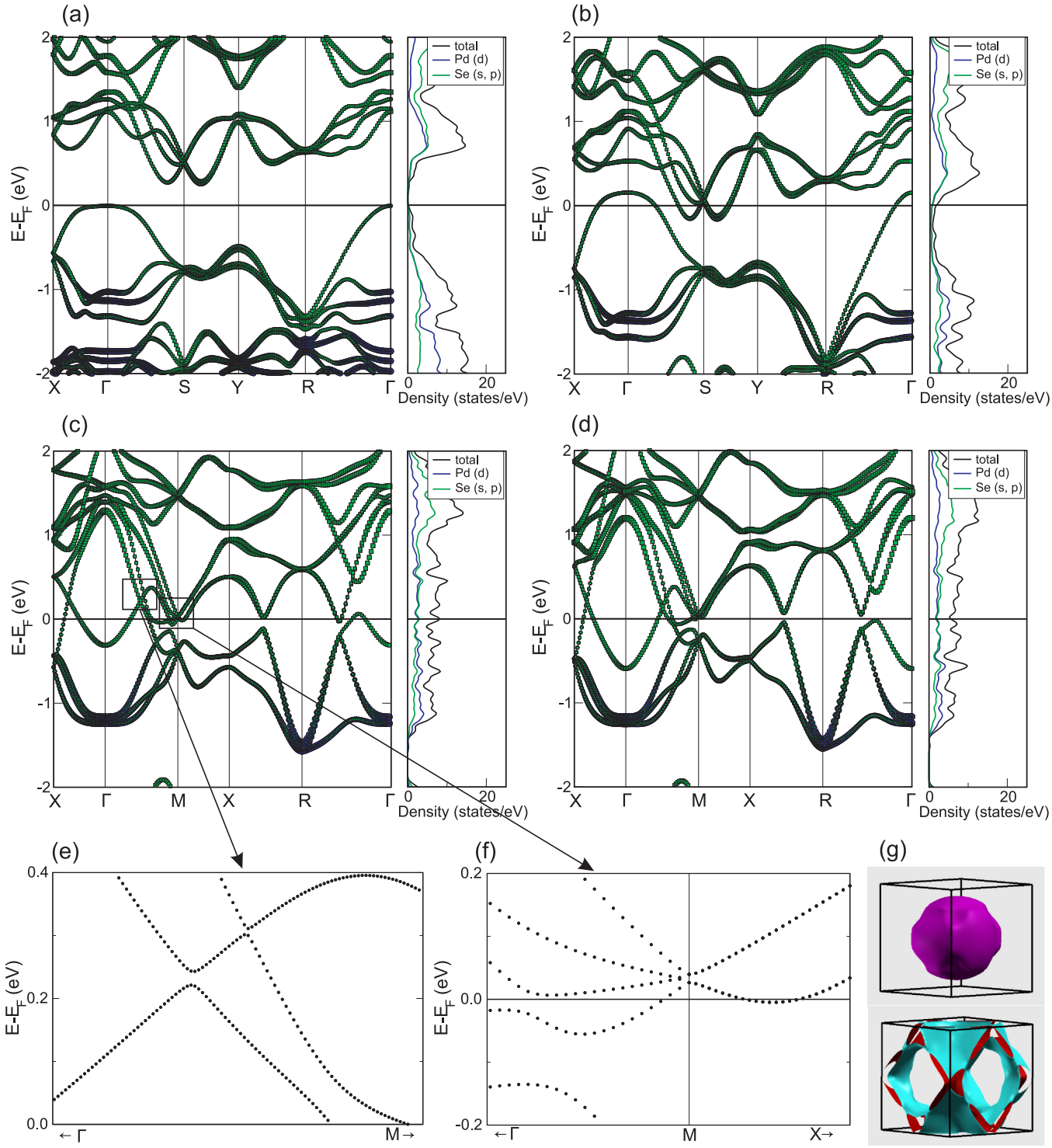

FIG. 3. Calculated electronic structure of $PdSe_2$. (a) The electronic band structure of the semiconducting PdS_2-type phase at ambient pressure. The valence band maximum at the Γ point has Pd d_{z^2} character hybridized with the p_z state of Se. The conduction band minimum is between the S and Y high-symmetry points and consists of Pd $d_{x^2-y^2}$ and Se p states. (b) At about 2 GPa the band structure shows the metallization of $PdSe_2$ with the PdS_2-type structure. (c) The electronic structure of $PdSe_2$ in the pyrite phase with bands crossing the Fermi energy is very different from that of the PdS_2-type structure. (d) A further increase of the pressure pushes the bands' extrema away from the Fermi energy. (e) Dirac crossing along the ΓM direction and two fourfold degeneracies separated by ∼0.01 eV at the M point near E_F (f) obtained including SOC. (g) The Fermi surface of the pyrite phase for the band structure (c). The network along the edges of the Brillouin zone (lower panel) is formed by small electron and hole pockets. At high pressure these bands move away from the E_F (d) and the Fermi surface will only contain the cubelike pockets.

temperature T_c increases rapidly, reaches a maximum of 13.1 K at ≈23 GPa, and then decreases continuously for higher pressures up to ≈37 GPa. The resistivity in the normal state shows a normal-metallic behavior upon heating up to room temperature at all pressures.

The Raman spectra of $PdSe_2$ in the pyrite phase display a remarkably nonmonotonous evolution of the frequencies of the librational E_g and internal stretching A_g modes with pressure [Fig. 1(c)]. Just after the transition to the pyrite phase, the frequency of the E_g mode increases with pressure, consistent with a shortening of the Pd-Se distance under compression. Concomitantly, the stretching vibration softens considerably, indicating the weakening of the Se-dimer bond likely governed by electronic correlations [27]. Both frequencies reach their extrema at a pressure above ≈22 GPa and then display the opposite trend with further increasing pressure. Figure 2(c) shows a clear correlation between the pressure dependences of T_c and the frequencies of the A_g and E_g modes which directly reflect the strengths of Se-Se and Pd-Se bonds in $PdSe_2$.

Quantitatively, the pressure effect on superconductivity may be expressed with the McMillan formula which connects T_c with a characteristic phonon frequency ω, the electron-phonon coupling parameter $\lambda = N(E_F)I^2/M\omega^2$ [where $N(E_F)$ is the electronic DOS at E_F, I^2 is the electron-ion matrix element, and M is the atomic mass], and the effective Coulomb repulsion μ^* [28]. By taking its logarithmic volume derivative,

$$\frac{d\ln T_c}{d\ln V} = -B\frac{d\ln T_c}{dP} \cong (2\Delta - 1)\gamma + \Delta\frac{d\ln\eta}{d\ln V}, \qquad (1)$$

where B is the bulk modulus, $\Delta \equiv 1.02\lambda[\lambda - \mu^* - \mu^*\lambda]^{-2}$, $\gamma \equiv -d\ln\omega/d\ln V$ is the Grüneisen parameter, and $\eta \equiv N(E_f)I^2$ is known as the Hopfield parameter [29,30]. The first term on the right-hand side of Eq. (1) expresses the effect of the change of the phonon frequency, whereas the second is an "electronic" term. Using the experimental data of the pressure dependence of T_c and ω in $PdSe_2$ and $B = 77.9$ GPa [19], it is evident that for any combination of λ and μ^* in the relevant ranges ($\lambda = 0.1$–2.0 and $\mu^* = 0$–0.2), the observed strong enhancement of T_c ($d\ln T_c/dP \approx 25\%$/GPa) cannot be explained by a softening of the A_g phonon frequency ($d\ln\omega/dP \approx -1.8\%$/GPa) alone and the electronic term in Eq. (1) appears to be the dominant factor.

Interestingly, $N(E_F)$ shows only a weak evolution with pressure [Figs. 3(c) and 3(d)] and cannot explain the strong increase of T_c. Within the McMillan formula, the remaining possibility is a significant enhancement of I^2, which might be driven by a pressure effect on the ionic polarizability of the Se-Se dimer. Pyrite TMDs are known for large polarizabilities [e.g., for NiS_2, the dielectric constant $\varepsilon_\infty \approx 26$, comparable with polarizabilities of organic superconductors ($\varepsilon_\infty \approx 20$) [31] and high-$T_c$ cuprates ($\varepsilon_\infty \approx 50$) [32], where dielectric properties play a significant role in the electron pairing] [33,34] which are caused by charge fluctuations due to the strong hybridization between the cation d states and the anion $sp\sigma^*$ states near the Fermi level [35]. As a result, the ionic polarizability screens out the electronic polarizability for states close to E_F, greatly modifying the Coulomb repulsion μ^*, and I^2 becomes very large for the screened states [36]. The gain in the intensity of the E_g mode [Fig. 1(c)] in $PdSe_2$ with increasing pressure is probably induced by resonance effects. It might be indicative for an enhancement of the oscillator strength of the virtual Pd $4d$–Se $4p$ transitions due to strengthening of the Pd-Se bonding and may cause an increase of the polarizability. Alternatively, the application of pressure increases the Se-Se distance R and consequently the ionic polarizability ($\alpha \sim R^2$) of the Se_2 dumbbell governing the strong enhancement of T_c. The dome-shaped dependence of T_c on pressure is conditioned by the competition of pressure-induced band broadening favoring enhancement of hybridization of Pd d−Se_2 $sp\sigma^*$ states, and the shift of the bands with an increasing difference between the bonding and antibonding states under compression [37], expelling at a certain pressure the antibonding $sp\sigma^*$ states of Se_2 dimers above E_F [Fig. 3(d)]. This leads to softening of Pd-Se and strengthening of Se-Se bonds, benchmarking the turning point of the pressure dependence of T_c.

In conclusion, the application of pressure leads to the emergence of superconductivity in the pyrite phase of $PdSe_2$, with T_c rapidly increasing in correlation with a weakening of Se-Se bonds. This is due to a charge transfer from the metal atoms to the antibonding states of the Se_2 dumbbell effectively oxidizing the Pd (d^8) to a higher oxidation state ($d^{8-\delta}$). The large family of transition-metal compounds with the pyrite structure offers a wide range of possibilities for tuning the oxidation state of the metal atoms and bonding strength of the dumbbells by chemical substitution, opening the perspective to achieve higher values of T_c and to eventually stabilize the superconducting state at ambient pressure. The presence of topological bands additionally allows probing the interplay between topological states and superconductivity, which can lead to different exotic superconducting states of matter in this crystal structure.

This work was financed by the Deutsche Forschungsgemeinschaft (DFG) under the Projects No. ME 3652/3-1 and No. GRK 1621 and by the European Union Horizon 2020 research and innovation program within the PETMEM project (Grant No. 688282). P.G.N. acknowledges the support by the Russian Science Foundation (Project No. 17-72-20200).

[1] P. C. Canfield, Nat. Mater. **10**, 259 (2011).

[2] E. Morosan, H. W. Zandbergen, B. S. Dennis, J. W. G. Bos, Y. Onose, T. Klimczuk, A. P. Ramirez, N. P. Ong, and R. J. Cava, Nat. Phys. **2**, 544 (2006).

[3] B. Sipos, A. F. Kusmartseva, A. Akrap, H. Berger, L. Forro, and E. Tutis, Nat. Mater. **7**, 960 (2008).

[4] A. F. Kusmartseva, B. Sipos, H. Berger, L. Forró, and E. Tutiš, Phys. Rev. Lett. **103**, 236401 (2009).

[5] Y. Qi, S. Matsuishi, J. Guo, H. Mizoguchi, and H. Hosono, Phys. Rev. Lett. **109**, 217002 (2012).

[6] J. Guo, Y. Qi, S. Matsuishi, and H. Hosono, J. Am. Chem. Soc. **134**, 20001 (2012).

[7] S. Jobic, R. Brec, and J. Rouxel, J. Alloys Compd. **178**, 253 (1992).
[8] J. A. Wilson and A. D. Yoffe, Adv. Phys. **18**, 193 (1969).
[9] Y. Feng, R. Jaramillo, A. Banerjee, J. M. Honig, and T. F. Rosenbaum, Phys. Rev. B **83**, 035106 (2011).
[10] G. W. Hull and F. Hulliger, Nature (London) **220**, 257 (1968).
[11] F. Hulliger, J. Phys. Chem. Solids **26**, 639 (1965).
[12] Y. Qi, P. G. Naumov, M. N. Ali, C. R. Rajamathi, W. Schnelle, O. Barkalov, M. Hanfland, S.-C. Wu, C. Shekhar, Y. Sun, V. Süß, M. Schmidt, U. Schwarz, E. Pippel, P. Werner, R. Hillebrand, T. Forster, E. Kampert, S. Parkin, R. J. Cava, C. Felser, B. Yan, and S. A. Medvedev, Nat. Commun. **7**, 10038 (2016).
[13] G. Kresse and J. Furthmüller, Phys. Rev. B **54**, 11169 (1996).
[14] P. E. Blöchl, Phys. Rev. B **50**, 17953 (1994).
[15] G. Kresse and D. Joubert, Phys. Rev. B **59**, 1758 (1999).
[16] J. Klimeš, D. R. Bowler, and A. Michaelides, J. Phys.: Condens. Matter **22**, 022201 (2010).
[17] J. Klimes, D. R. Bowler, and A. Michaelides, Phys. Rev. B **83**, 195131 (2011).
[18] A. A. Mostofi, J. R. Yates, G. Pizzi, Y.-S. Lee, I. Souza, D. Vanderbilt, and N. Marzari, Comput. Phys. Commun. **185**, 2309 (2014).
[19] C. Soulard, X. Rocquefelte, P. E. Petit, M. Evain, S. Jobic, J. P. Itié, P. Munsch, H. J. Koo, and M. H. Whangbo, Inorg. Chem. **43**, 1943 (2004).
[20] C. de las Heras and F. Agulló-Rueda, J. Phys.: Condens. Matter **12**, 5317 (2000).
[21] C.-K. Chiu and A. P. Schnyder, Phys. Rev. B **90**, 205136 (2014).
[22] G. Bian, T.-R. Chang, R. Sankar, S.-Y. Xu, H. Zheng, T. Neupert, C.-K. Chiu, S.-M. Huang, G. Chang, I. Belopolski, D. S. Sanchez, M. Neupane, N. Alidoust, C. Liu, B. Wang, C.-C. Lee, H.-T. Jeng, C. Zhang, Z. Yuan, S. Jia, A. Bansil, F. Chou, H. Lin, and M. Z. Hasan, Nat. Commun. **7**, 10556 (2016).
[23] G. Bian, T.-R. Chang, H. Zheng, S. Velury, S.-Y. Xu, T. Neupert, C.-K. Chiu, S.-M. Huang, D. S. Sanchez, I. Belopolski, N. Alidoust, P.-J. Chen, G. Chang, A. Bansil, H.-T. Jeng, H. Lin, and M. Z. Hasan, Phys. Rev. B **93**, 121113 (2016).
[24] S.-Y. Guan, P.-J. Chen, M.-W. Chu, R. Sankar, F. Chou, H.-T. Jeng, C.-S. Chang, and T.-M. Chuang, Sci. Adv. **2**, e1600894 (2016).
[25] B. Bradlyn, J. Cano, Z. Wang, M. G. Vergniory, C. Felser, R. J. Cava, and B. A. Bernevig, Science **353**, aaf5037 (2016).
[26] S. Friedemann, H. Chang, M. B. Gamża, P. Reiss, X. Chen, P. Alireza, W. A. Coniglio, D. Graf, S. Tozer, and F. M. Grosche, Sci. Rep. **6**, 25335 (2016).
[27] B. G. Jang, D. Y. Kim, and J. H. Shim, Phys. Rev. B **95**, 075144 (2017).
[28] W. L. McMillan, Phys. Rev. **167**, 331 (1968).
[29] T. Tomita, J. J. Hamlin, J. S. Schilling, D. G. Hinks, and J. D. Jorgensen, Phys. Rev. B **64**, 092505 (2001).
[30] I. Loa and K. Syassen, Solid State Commun. **118**, 279 (2001).
[31] K. Bender, K. Dietz, H. Endres, H. W. Helberg, I. Hennig, H. J. Keller, H. W. Schäfer, and D. Schweitzer, Mol. Cryst. Liq. Cryst. **107**, 45 (1984).
[32] D. Reagor, E. Ahrens, S. W. Cheong, A. Migliori, and Z. Fisk, Phys. Rev. Lett. **62**, 2048 (1989).
[33] D. Jérome, in *The Physics of Organic Superconductors and Conductors*, edited by A. Lebed (Springer, Berlin, 2008).
[34] B. P. P. Mallett, T. Wolf, E. Gilioli, F. Licci, G. V. M. Williams, A. B. Kaiser, N. W. Ashcroft, N. Suresh, and J. L. Tallon, Phys. Rev. Lett. **111**, 237001 (2013).
[35] W. Folkerts, G. A. Sawatzky, C. Haas, R. A. de Groot, and F. U. Hillebrecht, J. Phys. C: Solid State Phys. **20**, 4135 (1987).
[36] M. Weger, M. Peter, and L. P. Pitaevskii, Z. Phys. B: Condens. Matter **101**, 573 (1996).
[37] A. K. McMahan, Physica B+C **139**, 31 (1986).